Supporting Information: Investigating apparent differences between standard DKI and axisymmetric DKI and its consequences for biophysical parameter estimates

Jan Malte Oeschger[1] Karsten Tabelow[2] Siawoosh Mohammadi[1,3,4,*]

January 12, 2024

1 University Medical Center Hamburg-Eppendorf, Institute of Systems Neuroscience, Hamburg, Germany

2 Weierstrass Institute for Applied Analysis and Stochastics, Berlin, Germany

3 Max Planck Research Group MR Physics, Max Planck Institute for Human Development, Berlin, Germany

***** Corresponding author:

Name Siawoosh Mohammadi

Institute Max Planck Institute for Human Development, Max Planck Research Group MR Physics

Address Lentzeallee 94, 14195, Berlin

E-mail mohammadi@mpib-berlin.mpg.de

Phone +49 30 82406-0

Supporting Information

S1.1 Standard DKI signal representation

For a given diffusion weighting b and diffusion gradient $\vec{g} = (g_1, g_2, g_3)^\mathsf{T}$, the noise-free DKI signal can be represented as in [1;2]:

$$S_{b,\vec{g}}(S_0, D, W) = S_0 \exp\left[-bD + \frac{b^2}{6}\left(\frac{\mathrm{Tr}(D)}{3}\right)^2 W\right] \quad \text{[S1.1a]}$$

$$D = \sum_{i,j=1}^{3} g_i g_j D_{ij} \quad \text{[S1.1b]}$$

$$W = \sum_{i,j,k,l=1}^{3} g_i g_j g_k g_l W_{ijkl} \quad \text{[S1.1c]}$$

where D_{ij} are the diffusion tensor entries, W_{ijkl} are the kurtosis tensor entries and S_0 is the non-diffusion-weighted signal ($b = 0\frac{\mathrm{s}}{\mathrm{mm}^2}$).

From the tensors metrics in D and W, the AxTM can be directly computed: $D_\parallel = \lambda_1$ where λ_1 is the first eigenvalue of the diffusion tensor D, $D_\perp = \frac{\lambda_2+\lambda_3}{2}$. $W_\parallel$ and $W_\perp$ can be computed from the fitted W tensor according to formulas 11 and 12 from [4]: $W_\parallel = W(\nu_1) = W_{1111}$, where ν_1 is the first eigenvector of the corresponding diffusion tensor and $W_\perp = 3/8(W_{2222} + W_{3333} + 2W_{2233})$. $\overline{W}$ can be computed according to Eq. 10 from [5]: $\overline{W} = 1/5(W_{1111} + W_{2222} + W_{3333} + 2W_{1122} + 2W_{1133} + 2W_{2233})$ (in [5]: 1=x, 2=y, 3=z).

S1.2 Axisymmetric DKI

Axisymmetric DKI[4] assumes symmetric diffusion around an axis of symmetry $\vec{c}$ inside an imaging voxel. Mathematically, this assumption leads to axisymmetric diffusion and kurtosis tensors with a drastically reduced number of independent tensor parameters compared to standard DKI (from 15 to 3 parameters for the kurtosis tensor and from 6 to 2 parameters for the diffusion tensor). Apart from the tensors, axisymmetric DKI additionally contains two parameters for the axis of symmetry.

With the axis of symmetry $\vec{c}$ parameterized by the inclination θ and azimuth ϕ: $\vec{c} = \begin{pmatrix} \sin\theta\cos\phi \\ \sin\theta\sin\phi \\ \cos\theta \end{pmatrix}$, the diffusion and kurtosis tensors can be determined according to[4]:

$$D = D_\perp \mathbf{I} + (D_\parallel - D_\perp)\vec{c}\vec{c}^T \qquad \text{[S1.2]}$$

and

$$\begin{aligned} W =& \frac{1}{2}(10W_\perp + 5W_\parallel - 15\overline{W})\mathbf{P} + W_\perp \mathbf{\Lambda} + \\ & \frac{3}{2}(5\overline{W} - W_\parallel - 4W_\perp)\mathbf{Q} \end{aligned}$$

where $\Psi = \{D_\parallel, D_\perp, W_\parallel, W_\perp, \overline{W}, S_0, \theta, \phi\}$ are the 8 framework's parameters (S_0 is the non diffusion-weighted signal) and $\mathbf{I} = \begin{pmatrix} 1 & 0 & 0 \\ 0 & 1 & 0 \\ 0 & 0 & 1 \end{pmatrix}$ is the identity matrix. The tensors $\mathbf{P}, \mathbf{\Lambda}$ and $\mathbf{Q}$ can be computed with the Kronecker delta δ_{xy} and the components of the axis of symmetry c_x ($x, y \in$

$1,2,3$) as: $\mathbf{P}_{ijkl} = c_i c_j c_k c_l$, $\mathbf{Q}_{ijkl} = \frac{1}{6}(c_i c_j \delta_{kl} + c_i c_k \delta_{jl} + c_i c_l \delta_{jk} + c_j c_k \delta_{il} + c_j c_l \delta_{ik} + c_k c_l \delta_{ij})$ and $\mathbf{\Lambda}_{ijkl} = \frac{1}{3}(\delta_{ij}\delta_{kl} + \delta_{ik}\delta_{jl} + \delta_{il}\delta_{jk})$[4]. The according noise-free signal $S_{b,\vec{g}}(\Psi)$ can then be computed and fitted to dMRI data based upon the axisymmetric tensors[6]:

$$S_{b,\vec{g}}(\Psi) = S_0 \exp\left(-B_{ij}D_{ij} + \frac{1}{6}\overline{D}^2 B_{ij}B_{kl}W_{ijkl}\right) \quad [S1.3]$$

where

$$B_{ij}D_{ij} = \mathrm{Tr}(B)D_\perp + (D_\parallel - D_\perp)\vec{c}^T B\vec{c} \quad [S1.4]$$

and

$$B_{ij}B_{kl}W_{ijkl} = \frac{1}{2}(10W_\perp + 5W_\parallel - 15\overline{W})(\vec{c}^T B\vec{c})^2 \quad [S1.5]$$

$$+ \frac{1}{2}(5\overline{W} - W_\parallel - 4W_\perp)(\vec{c}^T B\vec{c}\,\mathrm{Tr}(B) \quad [S1.6]$$

$$+ 2\vec{c}^T BB\vec{c}) + \frac{W_\perp}{3}(Tr(B)^2 + 2\,\mathrm{Tr}(B\otimes B)) \quad [S1.7]$$

with

$$B = b\begin{pmatrix} g_x^2 & g_x g_y & g_x g_z \\ g_x g_y & g_y^2 & g_y g_z \\ g_x g_z & g_y g_z & g_z^2 \end{pmatrix}$$

Note that the AxTM can also be computed from the standard DKI tensor metrics assuming axial symmetry, see Section S1.1.

S1.3 Derivation of the relationship between the axisymmetric DKI tensor metrics and the biophysical parameters

The derivation of the relationship between the axisymmetric DKI tensor metrics and the biophysical parameters is based upon the work by[7;8]. Starting point for the derivation are the formulas found in[7] that establish a connection between the axisymmetric DKI tensor metrics and the biophysical parameters, based upon the assumption of an axially symmetric fiber orientation distribution function (ODF):

$$M_1 = 3D_0 = AWF \cdot D_a + (1 - AWF)(2D_{e,\perp} + D_{e,\parallel})$$
$$M_2 = \frac{3}{2}D_2\frac{1}{p_2} = AWF \cdot D_a + (1 - AWF)(D_{e,\parallel} - D_{e,\perp})$$
$$M_3 = D_2^2 + 5D_0^2(1 + \frac{W_0}{3}) = AWF \cdot D_a^2 + (1 - AWF)[5D_{e,\perp}^2 + (D_{e,\parallel} - D_{e,\perp})^2 + \frac{10}{3}D_{e,\perp}(D_{e,\parallel} - D_{e,\perp})]$$
$$M_4 = \frac{1}{2}D_2(D_2 + 7D_0)\frac{1}{p_2} + \frac{7}{12}\frac{1}{p_2}W_2D_0^2 = AWF \cdot D_a^2 + (1 - AWF)((D_{e,\parallel} - D_{e,\perp})^2 + \frac{7}{3}D_{e,\perp}(D_{e,\parallel} - D_{e,\perp}))$$
$$M_5 = \frac{9}{4}D_2^2 + \frac{35}{24}W_4D_0^2 = p_4(AWF \cdot D_a^2 + (1 - AWF)(D_{e,\parallel} - D_{e,\perp})^2)$$

M1, M2, M3, M4 and M5 only depend on the biophysical parameter κ via the functions p_2 and p_4 and the axisymmetric DKI tensor metrics $\overline{W}, W_\parallel, W_\perp, D_\parallel, D_\perp$:

$$D_0 = \frac{1}{3}(2D_\perp + D_\parallel) \qquad D_2 = \frac{2}{3}(D_\parallel - D_\perp)$$
$$W_0 = \overline{W} \qquad W_2 = \frac{1}{7}(3W_\parallel + 5\overline{W} - 8W_\perp)$$
$$W_4 = \frac{4}{7}(W_\parallel - 3\overline{W} + 2W_\perp)$$

$$p_2 = \frac{1}{4}(\frac{3}{\sqrt{\kappa}F(\sqrt{\kappa})} - 2 - \frac{3}{\kappa})$$
$$p_4 = \frac{1}{32\kappa^2}(105 + 12\kappa(5+\kappa) + \frac{5\sqrt{\kappa}(2\kappa - 21)}{F(\sqrt{\kappa})})$$

here, F is Dawsons function. A quadratic equation for AWF can be found (for detailed derivation see[8]):

$$0 = a \cdot AWF^2 - (a + c - \frac{40}{3})AWF + c \quad \text{[S1.8]}$$

where a and c are:

$$a = (\Delta m)^2 - (\frac{7}{3} + 2d_2)\Delta m + m_2 \quad \text{[S1.9]}$$

and:

$$c = (\Delta m - 5 - d_2)^2 \quad \text{[S1.10]}$$

that depend on d_2, m_2, $\overline{D}$ and Δm which can be computed with the axisymmetric DKI tensor metrics and κ:

$$\overline{D} = \frac{1}{3}(M_1 - M_2) \qquad \Delta m = \frac{M_3}{\overline{D}^2} - \frac{M_4}{\overline{D}^2}$$
$$d_2 := \frac{M_2}{\overline{D}} \qquad m_2 := \frac{M_4}{\overline{D}^2}$$

Eq. (S1.8) has two solutions referred to as "branches", which, in turn, can be computed with a and

c:

$$AWF_{-} = \frac{-\frac{40}{3} + a + c - \sqrt{-4ac + (\frac{40}{3} - a - c)^2}}{2a} \quad \text{[S1.11]}$$

$$AWF_{+} = \frac{-\frac{40}{3} + a + c + \sqrt{-4ac + (\frac{40}{3} - a - c)^2}}{2a} \quad \text{[S1.12]}$$

The solution for AWF (either branch "+" or "−") can then be used to compute the diffusivities $D_{e,\perp}$, $D_{e,\parallel}$ and D_a analytically.

$$D_{e,\perp} = \frac{\overline{D}}{(1 - AWF)} \qquad D_a = (\frac{\Delta m(1 - AWF) - 5 - d_2}{-AWF})\overline{D}$$
$$D_{e,\parallel} = (\frac{d_2 - AWF \cdot \frac{D_a}{\overline{D}}}{(1 - AWF)})\overline{D} + D_{e,\perp}$$

However, at this point κ is still unknown and needed to estimate p_2 and p_4. All the biophysical diffusion parameters and AWF can now be expressed in terms of κ and the axisymmetric DKI tensor metrics. This is used to define an objective function where κ is the only unknown parameter, since the axisymmetric DKI tensor metrics have previously been estimated:

$$0 = [p_4(AWF \cdot D_a^2 + (1 - AWF)(D_{e,\parallel} - D_{e,\perp})^2)] - M_5 \quad \text{[S1.13]}$$

This objective function is then minimized to find κ with which first AWF and then the biophysical diffusivites can be found as described. It was feasible to optimize this problem over a discrete, linearly sampled range of $[0 \leq \kappa \leq 50]$ because it depends on one non-negative parameter κ. This procedure was faster and more precise compared to using the available MATLAB solvers. There are at least two solutions[9;8] ("branches") to the optimization problem, but in the main paper only the results of the branch labeled "+" is reported. This branch choice corresponds to assuming

$4 - \sqrt{\frac{40}{3}} < \frac{D_a - D_{e,\parallel}}{D_{e,\perp}} < 4 + \sqrt{\frac{40}{3}}$ associated with $D_a > D_{e,\parallel}$ and also labeled $\eta = 1$ in[7] or $\zeta = +$ in[8] and is in line with existing literature[7;10;11;12] on the branch selection using the intra-axonal diffusivity as a deciding factor, see Section 4.2, main document, for a further discussion.

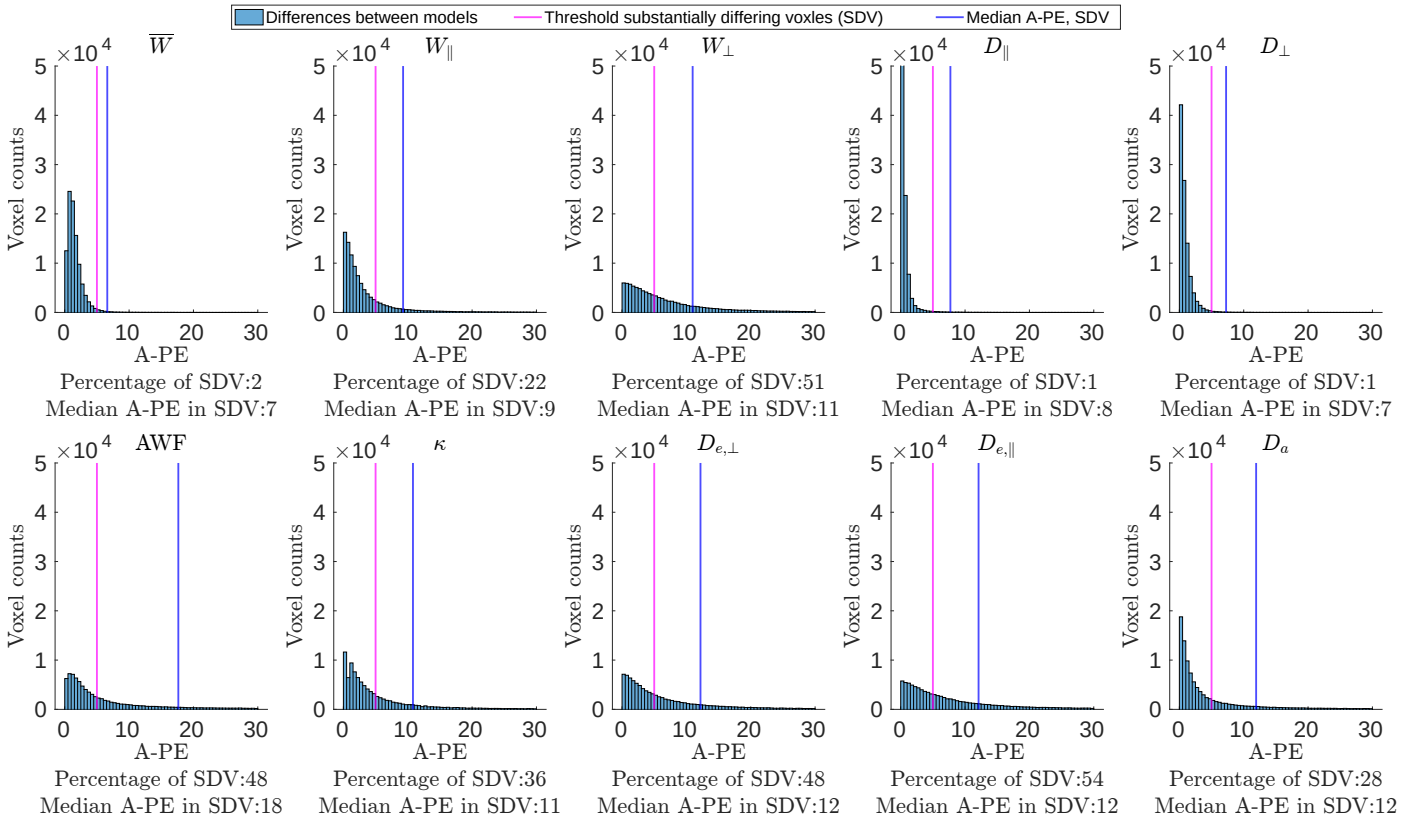

Figure S1: Histograms of underlying A-PE distribution for the AxTM and biophysical parameters. The pink vertical lines indicate the threshold after which axisymmetric DKI parameter estimation results were considered "substantially differing" (A-PE $\geq 5\%$), the blue vertical lines indicate the median difference in the population of substantially differing voxels. The x-axis was confined to [0 30].

S1.4 Histograms of A-PE for the AxTM and biophysical parameters

Because the main document cites the summary measures number of substantially differing voxels (SDV) and median bias in the population of SDV for brevity, Figure S1 shows the actual distributions of A-PE of the AxTM and biophysical parameters.

S1.5 Comparison of fit of log of signals with NLLS fit

An earlier work[13] has analytically shown that axisymmetric DKI and standard DKI should produce the same results if two pre-conditions are fulfilled: a) the log of the signals is being fitted and b) the axis of symmetry ($\vec{c}$) and the first eigenvector ($\vec{v_1}$), two measures for the main fiber orientation in

both DKI models, are identical. To rule out the possibility that the observed differences as measured by the A-PE between standard DKI and axisymmetric DKI in this study are caused by fitting the non-linear signals (pre-condition a)), a log-of-signals fit was implemented for both standard DKI and axisymmetric DKI and used to fit the same dMRI data described in Section 2.1 (main document). Figure S2 shows the difference between standard DKI and axisymmetric DKI when fitting the log-of-signals (orange histograms) versus the differences when using the NLLS fit implementation (blue histograms) at the top and the scatter density plots between the results obtained with both methods at the bottom.

Fitting the log of the signals still went along with substantial differences between both DKI models that in some cases, e.g., $W_{\perp}$, showed a close relation with the NLLS fit results. It can therefore be ruled out that the observed differences in the main study are purely caused by not fitting the log of the signals.

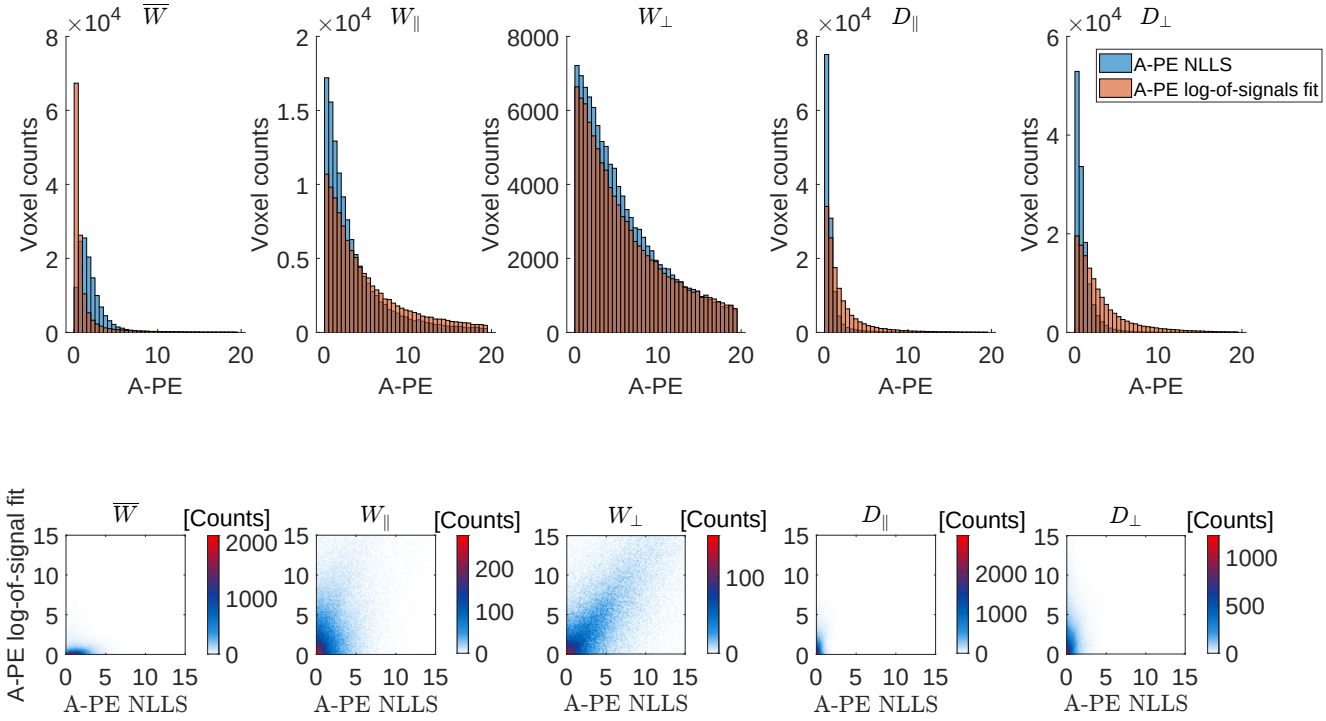

Figure S2: A-PE estimated based on a log-of-signals fit and the non-linear least sqaures (NLLS) fit used for this study. Top: histograms of A-PE distributions when fitting the log-of-signals (orange histograms) versus the NLLS fit implementation (blue histograms). Bottom: Scatter density plots of the A-PE estimated with a log-of-signals fit (y-axis) versus the NLLS fit (x-axis).

S1.6 Inter-dependence of A-PE and difference in main fiber orientation

It was analytically shown in[13] that standard DKI and axisymmetric DKI produce the same results under two conditions (see Section S1.5). Here, the pre-condition b) from Section S1.5 is investigated. To investigate a possible inter-dependency between the A-PE and the difference between $\vec{v_1}$ and $\vec{c}$, the angle ϕ between $\vec{v_1}$ and $\vec{c}$ was calculated according to: $\phi = \cos^{-1}(abs(\frac{\vec{v_1}\cdot\vec{c}}{|\vec{v_1}||\vec{c}|}))$ and plotted against the A-PE as a scatter density plot for each parameter, see Figure S3.

In almost all AxTM voxels the angle ϕ was greater 0° degree, see x-axes of Figure S3, indicating that the main fiber orientations estimated by both DKI models were almost never identical. This violates one of the necessary presumptions named in[13]. The scatter density plots in Figure S3 indicate that the kurtosis metrics $W_\perp$ and $W_\parallel$ had the highest inter-dependency between A-PE and ϕ allowing to establish at least a partial causality in this case.

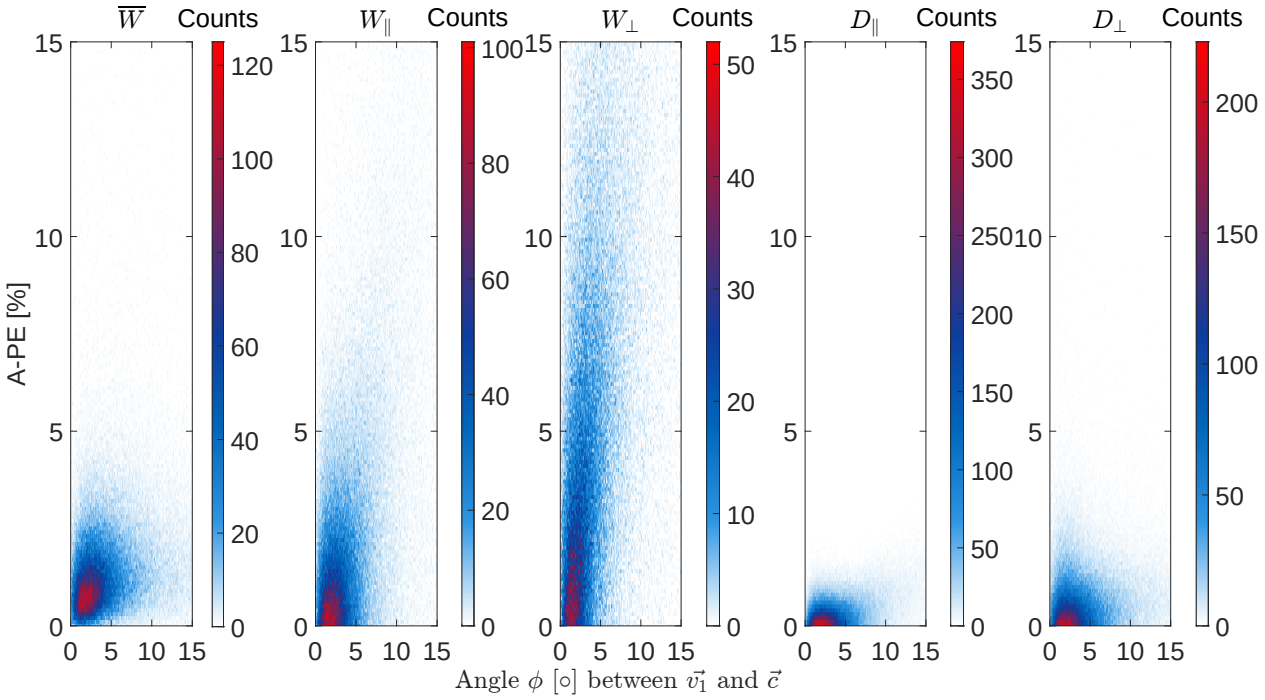

Figure S3: Scatter density plots between A-PE and angle ϕ computed for voxels in the white matter mask.

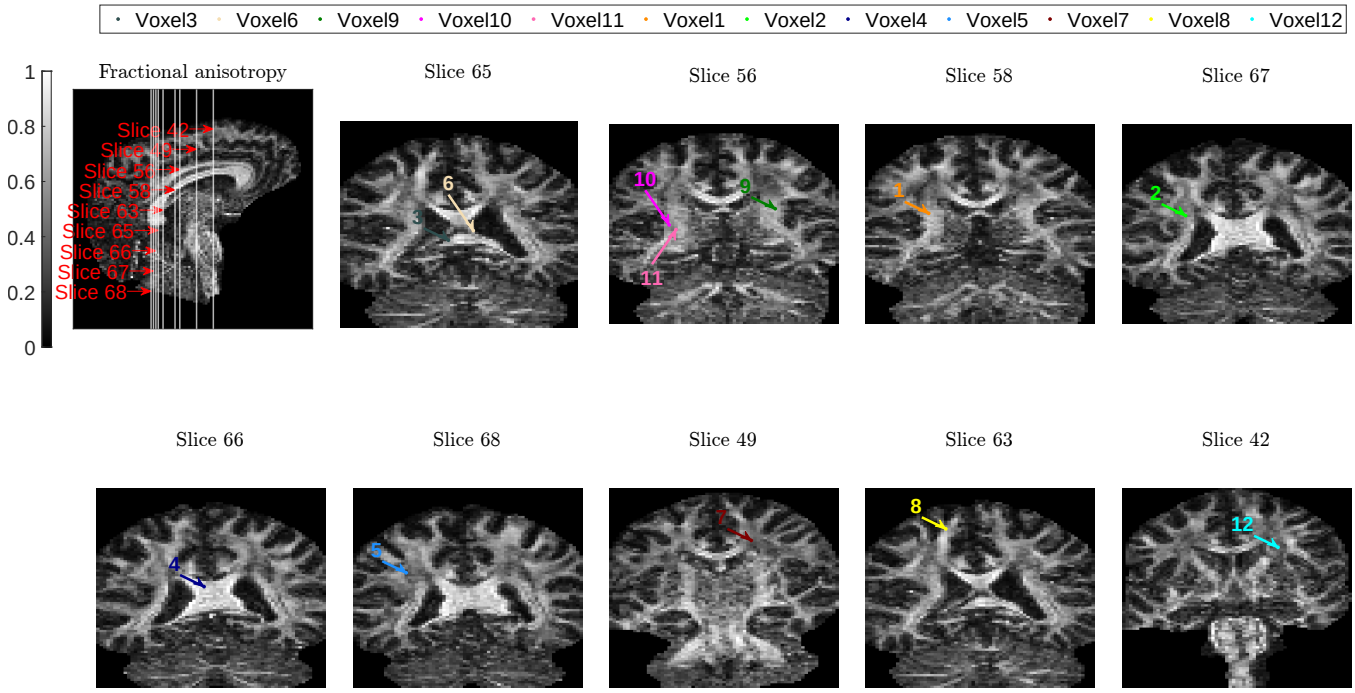

Figure S4: Voxel positions of the simulated voxels in the "single voxel analysis" corresponding to the parameters listed in Table S1 and Table S2. Top left image shows a sagittal overview of a fractional anisotropy image identifying the slices from which the voxels were extracted. The other images show the concrete voxel position in the according coronal slices.

S1.7 Ground truth datasets, single voxel analysis

Here, the ground truth datasets used to simulate the data of the single voxel analysis (see Section 2.4, main manuscript) are documented. Figure S4 shows the 12 selected voxels in the FA image of the human brain data used in this study. Table S1 and Table S2 document the corresponding ground truth diffusion and kurtosis tensor components and ground truth AxTM values.

Table S1: Ground truth datasets for the voxels simulated in the single voxel analysis (see Section 2.4, main document), shown are the diffusion and kurtosis tensor components and S_0, the diffusivities are in $[\frac{\mu m^2}{ms}]$.

Parameter	Voxel 1	Voxel 2	Voxel 3	Voxel 4	Voxel 5	Voxel 6
D_{11}	0.52518	0.73186	1.47547	1.59281	0.94294	1.35323
D_{22}	0.78697	0.74288	1.04926	0.28458	0.90303	0.00005
D_{33}	1.23249	1.18773	0.81426	0.42473	1.31293	0.66199
D_{12}	−0.11517	−0.03012	0.71930	0.19176	0.01800	0.11456
D_{13}	0.07573	0.17281	0.46296	0.54313	0.06349	−0.69321
D_{23}	−0.63971	−0.24029	0.17883	0.05975	0.17136	−0.10751
S_0	1.00000	1.00000	1.00000	1.00000	1.00000	1.00000
W_{1111}	0.67775	1.07929	1.22721	3.92558	1.16881	4.03335
W_{2222}	0.65740	0.93806	0.61860	0.51298	0.69336	−1.23230
W_{3333}	1.71966	1.25306	0.60559	−0.00206	1.34117	1.08392
W_{1112}	0.00302	0.06835	0.56475	0.30247	−0.02502	0.11231
W_{1113}	−0.02877	0.16450	0.25254	0.95462	0.21085	−2.10340
W_{2221}	−0.16901	−0.09296	0.48807	0.07772	0.04203	0.13599
W_{3331}	0.05064	0.04273	0.30247	0.38988	0.10736	−0.96426
W_{2223}	−0.21847	0.01396	0.02596	−0.00270	0.11575	0.30162
W_{3332}	−0.79489	−0.40981	0.13169	0.18746	0.19683	−0.26582
W_{1122}	0.27296	0.37678	0.69557	0.59812	0.18333	0.09223
W_{1133}	0.37894	0.17585	0.36908	0.50056	0.40884	1.18587
W_{2233}	0.63105	0.52844	0.42591	0.02421	0.48544	−0.12350
W_{1123}	−0.15648	−0.12087	0.11193	−0.00798	0.00510	−0.40817
W_{2213}	0.06741	0.20863	0.21401	0.14025	0.00056	0.06386
W_{3312}	−0.07199	−0.14695	0.18450	0.06740	0.14811	0.21569

Parameter	Voxel 7	Voxel 8	Voxel 9	Voxel 10	Voxel 11	Voxel 12
D_{11}	0.70021	0.37055	0.45038	0.71309	0.68214	0.62777
D_{22}	1.23004	1.09191	0.91982	0.67809	0.73508	1.18568
D_{33}	0.74326	1.01422	1.48194	1.29819	1.65466	0.64001
D_{12}	−0.03462	0.07976	0.02886	−0.08694	−0.14949	−0.00692
D_{13}	−0.05384	−0.09113	0.14072	−0.33201	−0.08331	0.16751
D_{23}	−0.14196	−0.35298	−0.62415	−0.24086	−0.40065	0.06892
S_0	1.00000	1.00000	1.00000	1.00000	1.00000	1.00000
W_{1111}	0.25736	0.29625	0.59465	0.61617	0.90990	0.72413
W_{2222}	1.29478	1.19521	0.79010	0.94335	0.57185	1.94369
W_{3333}	0.84182	1.13021	2.11612	1.71149	2.21282	0.89254
W_{1112}	−0.20589	−0.15870	−0.07156	−0.20480	−0.10260	−0.45005
W_{1113}	−0.09519	0.04410	0.11754	0.06422	−0.11515	0.23148
W_{2221}	0.08161	0.12204	0.14148	−0.00514	−0.15031	0.09221
W_{3331}	0.08907	−0.08658	0.16565	−0.48564	−0.10745	0.04541
W_{2223}	0.04681	−0.45644	−0.15422	−0.18872	−0.09809	0.17618
W_{3332}	−0.00168	−0.30874	−0.67320	−0.12712	−0.45940	0.09544
W_{1122}	0.48547	0.30077	0.17656	0.23455	0.26919	0.26294
W_{1133}	0.16228	0.17903	0.30837	0.44797	0.22822	0.04977
W_{2233}	0.19544	0.81838	0.57202	0.34830	0.49117	0.54980
W_{1123}	−0.07992	0.01297	−0.12377	−0.09888	−0.05498	−0.10805
W_{2213}	−0.11182	−0.16823	−0.11215	−0.06127	0.07760	0.10235
W_{3312}	−0.07009	0.00660	0.01548	−0.17444	−0.12436	0.00486

Table S2: Ground truth AxTM of the single voxel analysis, corresponding to the tensor components listed in Table S1, the diffusivities are in $[\frac{\mu m^2}{ms}]$.

Voxel	$D_\perp$	$D_\parallel$	$W_\perp$	$W_\parallel$	$\overline{W}$
Voxel 1	0.42174	1.70116	0.58537	2.86371	1.12414
Voxel 2	0.66092	1.34064	0.90280	1.96013	1.08651
Voxel 3	0.57898	2.18102	0.45733	2.90384	1.08651
Voxel 4	0.23493	1.83226	0.09464	4.54115	1.33646
Voxel 5	0.88698	1.38493	0.82815	1.70754	1.07171
Voxel 6	0.10993	1.79541	−0.43832	6.96149	1.23884
Voxel 7	0.70221	1.26909	0.49554	1.14350	0.81607
Voxel 8	0.52738	1.42193	0.71850	2.65236	1.04360
Voxel 9	0.47971	1.89272	0.56223	2.78642	1.12295
Voxel 10	0.59895	1.49148	0.72198	2.03711	1.06653
Voxel 11	0.63328	1.80533	0.73628	2.56648	1.13435
Voxel 12	0.62942	1.19462	0.67564	2.03629	1.05708

References

[1] J. H. Jensen and J. A. Helpern, "Quantifying non-Gaussian water diffusion by means of pulsed-field-gradient MRI.," *Proceedings of ISMRM 2003, program number 2154*, 2003.

[2] J. H. Jensen, J. A. Helpern, A. Ramani, H. Lu, and K. Kaczynski, "Diffusional kurtosis imaging: The quantification of non-Gaussian water diffusion by means of Magnetic Resonance Imaging," *Magnetic Resonance in Medicine*, vol. 53, no. 6, pp. 1432–1440, 2005.

[3] A. Tabesh, J. H. Jensen, B. A. Ardekani, and J. A. Helpern, "Estimation of tensors and tensor-derived measures in diffusional kurtosis imaging," *Magnetic Resonance in Medicine*, vol. 65, no. 3, pp. 823–836, 2011.

[4] B. Hansen, N. Shemesh, and S. N. Jespersen, "Fast imaging of mean, axial and radial diffusion kurtosis," *NeuroImage*, vol. 142, pp. 381–393, Nov. 2016.

[5] B. Hansen, T. E. Lund, R. Sangill, and S. N. Jespersen, "Experimentally and computationally fast method for estimation of a mean kurtosis," *Magnetic Resonance in Medicine*, vol. 69, no. 6, pp. 1754–1760, 2013.

[6] B. Hansen, A. R. Khan, N. Shemesh, T. E. Lund, R. Sangill, S. F. Eskildsen, L. Østergaard, and S. N. Jespersen, "White matter biomarkers from fast protocols using axially symmetric diffusion kurtosis imaging," *NMR in Biomedicine*, vol. 30, no. 9, p. e3741, 2017.

[7] S. N. Jespersen, J. L. Olesen, B. Hansen, and N. Shemesh, "Diffusion time dependence of microstructural parameters in fixed spinal cord," *NeuroImage*, vol. 182, pp. 329–342, 2018.

[8] D. S. Novikov, J. Veraart, I. O. Jelescu, and E. Fieremans, "Rotationally-invariant mapping of

scalar and orientational metrics of neuronal microstructure with diffusion MRI," *NeuroImage*, vol. 174, pp. 518 – 538, 2018.

[9] I. O. Jelescu, J. Veraart, E. Fieremans, and D. S. Novikov, "Degeneracy in model parameter estimation for multi-compartmental diffusion in neuronal tissue," *NMR in biomedicine*, vol. 29, pp. 33–47, Jan. 2016.

[10] N. Kunz, A. R. da Silva, and I. O. Jelescu, "Intra- and extra-axonal axial diffusivities in the white matter: Which one is faster?," *NeuroImage*, vol. 181, pp. 314–322, Nov. 2018.

[11] A. F. Howard, M. Cottaar, M. Drakesmith, Q. Fan, S. Y. Huang, D. K. Jones, F. J. Lange, J. Mollink, S. U. Rudrapatna, Q. Tian, K. L. Miller, and S. Jbabdi, "Estimating axial diffusivity in the NODDI model," *NeuroImage*, vol. 262, p. 119535, Nov. 2022.

[12] B. Dhital, M. Reisert, E. Kellner, and V. G. Kiselev, "Intra-axonal diffusivity in brain white matter," *NeuroImage*, vol. 189, pp. 543–550, Apr. 2019.

[13] S. Nørhøj Jespersen, "White matter biomarkers from diffusion MRI," *Journal of Magnetic Resonance*, vol. 291, pp. 127–140, June 2018.